Design-oriented modelling for the synthesis of Cu nanoparticles by a RF thermal plasma: impact of quenching solutions, radiative losses and thermophoresis

S. Bianconi[1], M. Boselli[1], M. Gherardi[1] and V. Colombo[1]

[1]*Department of Industrial Engineering, Alma Mater Studiorum-Università di Bologna, Bologna, Italy*

Abstract: A numerical model for the simulation of the copper nanoparticles synthesis process by an induction thermal plasma system has been developed, taking into account the joint effects of radiative losses from the metallic vapour and thermophoretic transport of the synthetized nanoparticles on the process performance, for different reaction chamber geometries combined with different quench gas injection strategies and different power levels, in order to evaluate the impact of these phenomena in process design strategies.

Keywords: Thermal plasma modelling, thermophoresis, ICP, nanoparticle synthesis.

1. Introduction

Radio-frequency inductively coupled plasma (RF-ICP) technology has proven to be a viable means for continuous production of nanoparticles (NP), thanks to its distinctive features, such as high energy density, high chemical reactivity, high process purity, large plasma volume, precursors long residence time and high cooling rate (10^4–10^5 Ks^{-1}) in the tail of the plasma. The large number of process variables (e.g. frequency, power, process gases, phase of the precursor and system geometry) gives it a high versatility that comes at a price: process optimization (in terms of yield and size distribution of the NP) is a challenging task that can hardly rely on try & fail experimental approaches due to equipment costs and to the limited amount of information that can be obtained from conventional diagnostic techniques. Therefore, process optimization of the NP synthesis process in RF-ICP systems has to rely extensively on modelling techniques.

In this work, we report on design-oriented modelling for the optimization of an RF-ICP synthesis process of Cu NP starting from a solid precursor, taking into account the effect of: i) the geometry of the volume downstream the plasma source where NP are formed and grow (reaction chamber); ii) the injection of gas in the reaction chamber that affects flow fields, temperature distributions, cooling rates and particle deposition at the chamber walls, which must be minimized (quenching strategy). The adoption of a porous quench wall solution in a cylindrical chamber can be considered as an ‘‘active’’ quenching while the use of a shroud gas in the top part of a conical chamber instead can be considered as a “passive” quenching. The injection of quench gas from the porous wall should limit the amount of nanoparticles deposited on its surface [4]; in order to model this phenomenon, a sticking coefficient was introduced in the particle balance equation at the wall, investigating its effect with values ranging from 0% to 100%. The adopted simulative model can describe plasma thermo-fluid dynamics, electromagnetic fields, precursor trajectories and thermal history, and nanoparticle nucleation and growth. Radiative losses from Cu vapour and their effect on the precursor evaporation efficiency have also been taken into account in the model. Thermophoresis of nanoparticles is also included in the model, [5] as it increases the deposition of nanoparticles on the chamber walls, with a detrimental effect on process yield

2. Results

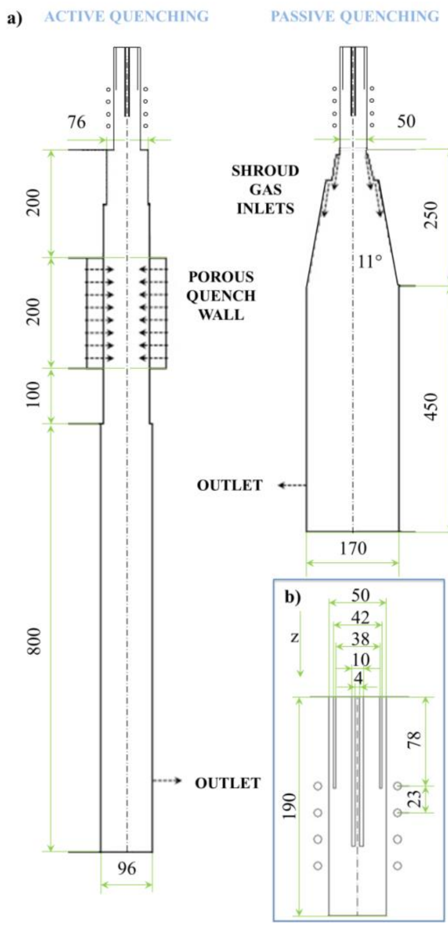

Fig. 1 Schematic of the reaction chambers (a) and of the torch (b). Dimensions are in mm [10].

The ICP nanoparticle synthesis process, including plasma thermo-fluid dynamics, electromagnetic field, precursor injection and evaporation, and nanoparticle formation, transport and growth, is modelled within a 2D axisymmetric framework in the ANSYS FLUENT© environment. The employed model describes plasma thermo-fluid dynamics, electromagnetic field, precursor behaviour (injection, trajectories, thermal history and evaporation) and nanoparticle formation, transport and growth. The employed model is described in [3] and [5], including all the assumptions and equations, as well as the computational domain (Figure 1), material properties and operating conditions.

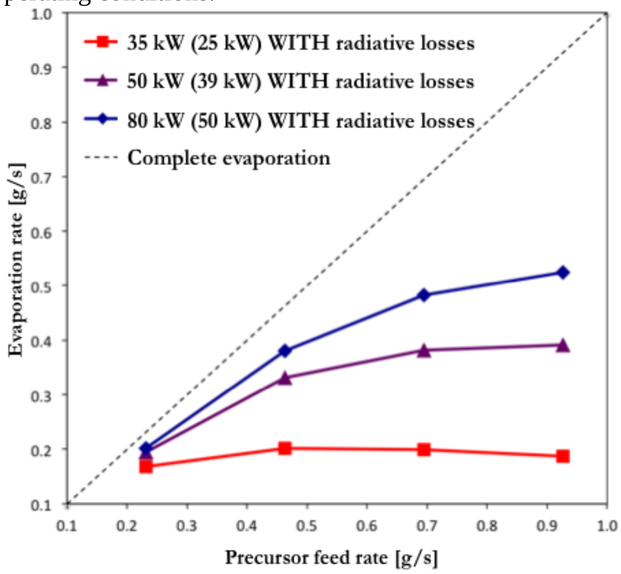

Fig. 2 Evaporation rates as a function of precursor feed rate for different plate power levels, taking into account radiative power losses from Cu vapour [3].

The evaporation rates and efficiencies as a function of precursor feed rate are reported in Figure.2 for three different plate power levels (35, 60 and 80 kW, corresponding to coupled power of 25, 39 and 50 kW, respectively). Complete evaporation of the precursor injected (up to 1 g/s of feed rate) was obtained for all three power levels in the simulations carried out without taking into account the radiative losses from Cu vapour (non-realistic conditions). Only in the case of 35 kW plate power level (25 kW coupled power), the precursor evaporation rate decreases when the precursor feed rate is increased over 0.46 g/s as a consequence of the *loading effect*. Conversely, the evaporation efficiency (Table 1) is significantly lower when including the radiative losses from Cu vapour, with a more pronounced decrease for higher precursor feed rates. Higher evaporation efficiency can be achieved adding a thermally insulated wall section at the top of the cylindrical chamber in order to maintain higher temperatures in the region of precursor evaporation [3].

This effect is more relevant for higher precursor feed rates: for instance for the case at 60 kW plate power (39 kW coupled power) for 0.93 g/s precursor feed rate the evaporation efficiency increases from 42% of the injected precursor to 54%.

Table 1. Evaporation efficiencies as a function of precursor feed rate for three different plate power levels (35, 60 and 80 kW, corresponding to 25, 39 and 50 kW coupled power, respectively), taking into account radiative power losses from Cu vapour [3].

Plate power (coupled power)	Precursor feed rate [g/s]			
	0.23	**0.46**	**0.69**	**0.93**
35 kW (25 kW)	73%	44%	29%	20%
60 kW (39 kW)	84%	72%	55%	42%
80 kW (50 kW)	87%	82%	69%	57%

The process yield, defined as the ratio between the total nanoparticle throughput and the precursor feed rate, and mean diameter of the synthetized nanoparticles have been calculated for different quench gas flow rates and using different sticking coefficients to model the particle deposition on the porous wall section [3]. The simulations were performed for the cases at 60 kW plate power (39 kW coupled power) and 0.46 g/s precursor feed rate. Table 2 reports the yield and mean diameter of synthetized nanoparticle for the case of a conical reaction chamber with 500 slpm of shroud gas (250 slpm for each of the two inlet regions), compared to the corresponding case in the cylindrical chamber, with 500 slpm quench gas flow rate and 50% sticking coefficient on the porous wall section. The synergic effect of the geometry and shroud gas in the conical chamber allows achieving both a high process yield (48%) and a low particle diameter (77 nm). Conversely, the quench gas injection in the cylindrical chamber does not positively affect the process yield, due to turbulent diffusion phenomena, as discussed in [3].

Table 2. Yield and mean diameter of the synthetized nanoparticles for the both the case without quench gas and with 500 slpm quench gas flow rate. All simulations were carried out for 60 kW plate power (39 kW coupled power) and a precursor feed rate of 0.46 g/s [3].

Chamber	**Quench**	**Yield (%)**	**$\bar{d}_P$ at outlet (nm)**
Cylindrical	No	11%	116
	500 slpm	11%	81
Conical	No	16%	87
	500 slpm	48%	77

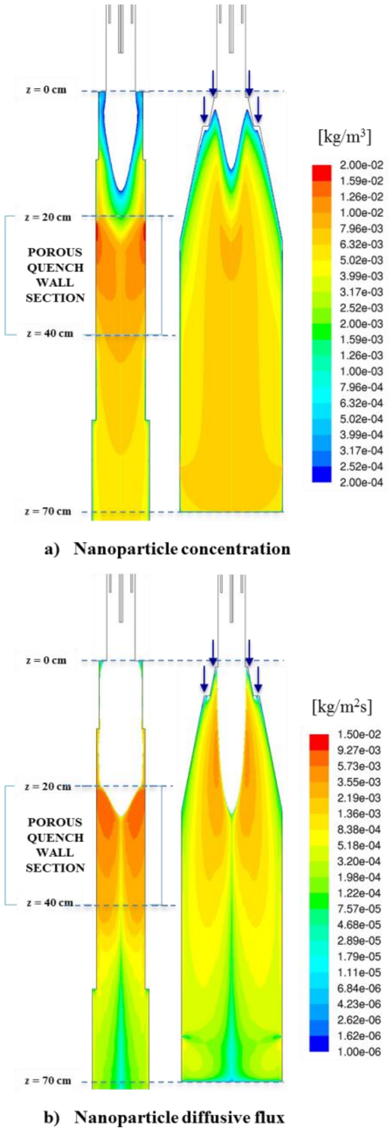

Fig. 3 Nanoparticles concentration (a) and nanoparticle radial diffusive flux towards the walls (b) for the cases of the cylindrical chamber (left) and the conical chamber (right) Both simulations were carried out for the case of 60 kW plate power (39 kW coupled power), 500 slpm of quench gas flow rate and 0.46 g/s precursor feed rate [3].

The nanoparticle concentration (displayed in Figure 3a) is peaked on the porous wall for the case of the cylindrical chamber, while it is peaked on the axis and low in proximity of the walls for the case of the conical chamber, thanks to the effect of the shroud gas flow. Similarly, the diffusive flux towards the walls (shown in Figure 3b) is lower in the conical chamber compared to the cylindrical chamber. A higher nanoparticle yield is thus achieved in the case of a conical chamber with 500 slpm shroud gas flow rate, as a result of a lower particle loss through deposition on the chamber walls.

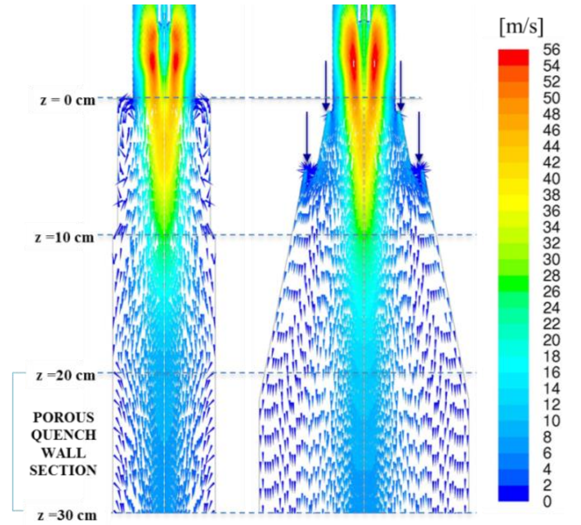

Fig. 4 Vector velocity fields for the cases of the cylindrical chamber (left) and the conical chamber (right). Both simulations were carried out for the case of 60 kW plate power (39 kW coupled power), 500 slpm of quench gas flow rate and 0.46 g/s precursor feed rate [3].

Velocity field vectors are reported in Figure 4 for each reaction chamber. In the cylindrical chamber vortices are generated close to the outlet of the plasma torch and below the porous quench wall section. These vortices affect PSD by increasing the particle mean size and have negative effect on the yield, as they increase the residence time of the powders in the chamber and the amount of powders lost to the walls. On the other hand, the conical chamber presents a laminar behavior with no notable vortices. Even with the same flow rate, the injection velocity of the quench gas coming from the porous wall is considerably lower than the shroud gas one. In the cylindrical chamber vortices are generated close to the outlet of the plasma torch and below the porous quench wall section. These vortices affect PSD by increasing the particle mean size and have negative effect on the yield, as they increase the residence time of the powders in the chamber and the amount of powders lost to the walls. On the other hand, the conical chamber presents a laminar behavior with no notable vortices.

Figure 5 shows the profiles of the vapour consumption by nucleation and condensation of the nanoparticles, together with the details of the thermophoretic particle flux, in the two chambers: these mechanisms are both localized in the upper region of the chamber, as both are connected to the cooling of the plasma. The steep temperature gradients that allow the quenching of the metallic vapour in the plasma and the consequent formation and growth of the nanoparticles, are also consistent with strong thermophoretic forces in such regions. Therefore, even in the upper region of the chamber there is a reduction of the nanoparticle concentration and axial flux due to thermophoresis.

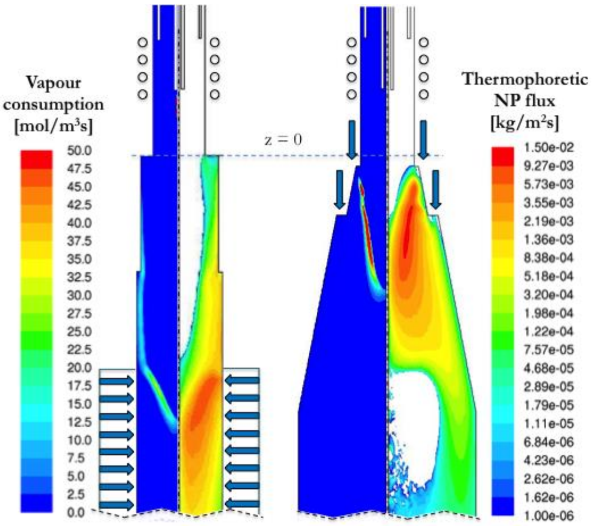

Fig. 5 Vapour consumption in the chamber by nucleation and condensation of nanoparticles (left half) and nanoparticle thermophoretic flux (right half) in the two chambers for 1000 slpm quench gas flow rate (500 slpm for each inlet in the conical chamber). Simulations were carried out for 60 kW plate power (39 kW coupled power) and a precursor feed rate of 0.46 g/s [5].

Table 3. Summary of the synthesis process performances in the two chambers, with and without the effect of the thermophoresis, for two power levels. The simulations were carried out for 1000 slpm quench gas flow rate (using 50% sticking coefficient to model the particle deposition on the porous wall in the cylindrical chamber) and a precursor feed rate of 0.46 g/s.

Chamber	Plate power (coupled power)	Thermo-phoresis	Yield (%)	$\bar{d}_P$ at outlet (nm)
Cylindrical	60 (39) kW	No	22%	71
		Yes	17%	65
	80 (50) kW	No	17%	59
		Yes	12%	52
Conical	60 (39) kW	No	42%	66
		Yes	38%	64
	80 (50) kW	No	49%	65
		Yes	46%	64

Table 3 reports the comparison of the effects induced by thermophoresis on the quenched process performances for two power levels compared (60 and 80 kW plate power, 39 and 50 kW coupled power). In the cylindrical chamber with active quenching the increase in power level has a detrimental effect on the process yield, and the effect of thermophoresis is also more intense, due to the stronger thermal gradients generated. Conversely, in the conical chamber with passive quenching, the increase in power level results in a higher process yield, probably thanks to a higher efficiency in the evaporation of the precursors (82 % [5]), while thermophoresis reduces its negative effect on yield, as well as it also reduces the positive effect on mean particle size.

3. Conclusions

The design-oriented modelling approach adopted in the present work allowed to gain insights on some of the phenomena governing the nanoparticle synthesis process, providing guidance towards the optimization and upscaling of the process, as an alternative to expensive try and fail experimental approaches. Radiation losses from the Cu vapour, when correctly included in the model, induce a significant reduction of the temperature observed in the region downstream the injection probe, resulting in a lower evaporation efficiency for the injected solid micrometric precursor. A comparison between two different chamber designs and quenching strategies is offered, with regards to the yield of the synthetized nanoparticles: the porous quench wall solution in a cylindrical can determine nanoparticle deposition losses due to turbulent diffusion that causes a low production yield. The use of a shroud gas in a conical chamber can instead reach much higher nanoparticle yield, which is a most important industrial target. Thermophoresis was shown to play an important role in the transport of the nanoparticles, in particular in the regions where steep temperature gradients exist, leading to a reduction in the process yield and a smaller particle mean diameter. The effect of thermophoresis is less detrimental on the yield when a quench gas is employed, especially in the case of a conical chamber with a passive quenching strategy.
Although the effects of the above-mentioned phenomena are strongly dependent on the properties of the material to be synthetized, the results shown in the present work can nonetheless be extended to different materials and operating conditions, in particular for the synthesis of metallic nanoparticles by an ITP system.

4. Acknowledgments

Work supported by European Union’s Horizon 2020 research and innovation program under grant agreement No 646155 (INSPIRED project).

5. References

[1] V Colombo, E. Ghedini, M. Gherardi, P. Sanibondi Plasma Sources Sci. Technol. **21** 055007 (2012).
[2] M. I. Boulos Plasma Chem Plasma Process. **36**, 3 (2016).
[3] S. Bianconi, M.Boselli, M. Gherardi, V. Colombo, Plasma Chem. Plasma Process., **37**, 3(2017)
[4] J. F. Bilodeau, P. Proulx, Aerosol Sci. Technol., **24**, 175 (1996).
[5] S. Bianconi, M.Boselli, M. Gherardi, V. Colombo, J. Phys. D. Appl. Phys. **50**, 16 (2017).